Optik 139 (2017) 291–298

Contents lists available at ScienceDirect

Optik

journal homepage: www.elsevier.de/ijleo

Original research article

Enhanced photovoltaic performance using reduced graphene oxide assisted by triple-tail surfactant as an efficient and low-cost counter electrode for dye-sensitized solar cells

A.B. Suriani[a,b,*], M.D. Nurhafizah[a,b], A. Mohamed[a,c], M.H. Mamat[d], M.F. Malek[e], M.K. Ahmad[f], A. Pandikumar[g], N.M. Huang[h]

[a] *Nanotechnology Research Center, Faculty of Science and Mathematics, Universiti Pendidikan Sultan Idris, 35900 Tanjung Malim, Perak, Malaysia*
[b] *Department of Physics, Faculty of Science and Mathematics, Universiti Pendidikan Sultan Idris, 35900 Tanjung Malim, Perak, Malaysia*
[c] *Department of Chemistry, Faculty of Science and Mathematics, Universiti Pendidikan Sultan Idris, 35900 Tanjung Malim, Perak, Malaysia*
[d] *NANO-ElecTronic Centre (NET), Faculty of Electrical Engineering, Universiti Teknologi MARA (UiTM), 40450 Shah Alam, Selangor, Malaysia*
[e] *NANO-SciTech Centre (NST), Institute of Science (IOS), Universiti Teknologi MARA (UiTM), 40450 Shah Alam, Selangor, Malaysia*
[f] *Microelectronic and Nanotechnology—Shamsuddin Research Centre (MiNT-SRC), Faculty of Electrical and Electronic Engineering, Universiti Tun Hussein Onn Malaysia, 86400 Parit Raja, Batu Pahat, Johor, Malaysia*
[g] *SRM Research Institute & Department of Chemistry, SRM University, SRM Nagar, Kattankulathur, 603 203, Tamil Nadu, India*
[h] *Low Dimensional Materials Research Centre, Department of Physics, Faculty of Science, University of Malaya, 50603 Kuala Lumpur, Malaysia*

ARTICLE INFO

Article history:
Received 9 January 2017
Accepted 5 April 2017

Keywords:
Reduced graphene oxide
Energy conversion
Dye-sensitized solar cell
Nanomaterials
Counter electrode

ABSTRACT

In this work, 4-bis(neopentyloxy)-3-(neopentyloxycarbonyl)-1,4-dioxobutane-2-silphonate (TC14) surfactant assisted reduced graphene oxide (rGO) was used as a counter electrode (CE) in dye-sensitized solar cell (DSSC). Field emission scanning electron microscopy and high-resolution transmission electron microscopy observations revealed that the TC14-rGO film was well dispersed on fluorine-doped tin oxide surface. The TC14-rGO modified CE based DSSC showed a power conversion efficiency of 0.828%, a short current density (J_{SC}) of 2.72 mA cm^{-2}, an open circuit voltage (V_{OC}) of 0.65 V, and a fill factor (FF) of 41.9 which were higher than those CE fabricated from commercially available SDS surfactant assisted rGO. Results revealed that TC14-rGO is a potential CE material to construct efficient DSSC for future solar cell applications.

1. Introduction

As an alternative renewable energy, solar energy has been extensively developed to slowly replace conventional energy sources, such as fossil fuels. Solar cells are considered an important device to convert solar energy to electricity power directly. In solar cell groups, dye-sensitized solar cells (DSSC) have been widely explored owing to the advantages, such as reasonable

* Corresponding author at: Nanotechnology Research Center, Faculty of Science and Mathematics, Universiti Pendidikan Sultan Idris, 35900 Tanjung Malim, Perak, Malaysia.
E-mail address: absuriani@yahoo.com (A.B. Suriani).

http://dx.doi.org/10.1016/j.ijleo.2017.04.025
0030-4026/

conversion efficiency, simple fabrication, low-cost, weak toxicity, flexibility, and light weight [1]. The DSSC comprise three main components: a transparent conductive glass as a photoanode (titanium dioxide, zinc oxide and tin oxide), a catalytic counter electrode (CE) as a cathode (platinum (Pt) or carbon), and a redox couple as an electrolyte (trioxide/iodide) [2]. A CE is an important component to regenerate a photosensitizer or dye, after an electron is injected; this component can then act rapidly to reduce the overall potential. The Pt-based CE in DSSC has also been introduced because of its high catalytic activity and chemical stability toward I^-/I_3^- electrolyte [1,3]. However, with high costs of Pt (~$1456 per Troy ounce at present) [3], tremendous effort have been taken to develop cost-effective CEs for DSSC and thus reduce the fabrication cost of device [4–6].

Carbon-based materials, such as carbon nanotubes (CNTs), are established as a CE materials for the photovoltaic enhancement in DSSC. Synthesized CNTs usually retain defect sites that act as an extra electron for kinetic transfer [7] rarely caused by functionalization and treatment processes [8]. These defects are also necessary to improve the DSSC performance. However, a complex technology should be developed because of costly and limited CNTs production. New carbon materials, graphene has excellent properties such as low charge transfer resistance, high surface-to-volume ratio, high chemical resistance, high carrier mobility, and high catalytic activity, which are suitable for the high performance and long-term stability of DSSC [1,9,10]. A two-dimensional honeycomb lattice material, graphene is considered as a potential candidate for Pt-free CE for DSSC. Graphene is synthesized by using top-to-down or bottom-to-up approaches that offer low-cost production. Solution-processing methods, such as electrochemical exfoliation, are more favourable than chemical vapour deposition because the former can be used for green and scalable production of single and multiple graphene layers in dispersions at low temperatures [11]. The functionalization and hybridization of graphene can be easily altered through solution-based approaches because functionalized graphene can provide more active sites for electron transfer kinetics in photovoltaic studies.

A calculated efficiency of approximately 2.8% is obtained for graphene −based materials as CE in DSSC [12]. In addition, photovoltaic measurements have been greatly enhanced after reduction of GO into rGO by using various amounts of hydrazine as reducing agents [13]. This phenomenon confirms that the density of introduced defects generates more active sites on the surface of reduced graphene oxide (rGO) based CE thus enhanced the DSSC performance [14]. Xu et al. also demonstrated the important role of other impurities or groups, such as NCHO in the functionalized rGO; as a result, its catalytic activity is higher than that of pristine graphene and rGO [15]. They found that oxygen-containing functional groups in graphene can enhance the catalytic performance of a DSSC device because edge sites promote a faster electron movement than basal sites do [16]. Thus, suitable synthesis methods for graphene production should be selected to maintain the catalytic performance percentage of oxygen-containing groups. The GO is reduced to rGO through chemical reduction, and this process is favourable because of its controllable production, convenience, and rapid reaction that can result in a massive amount of rGO in dispersions [17]. A surfactant is utilized as a stabilizer to stabilize rGO sheets in an aqueous solution because of a high van der Waals interaction between graphitic structures. Among various CE fabrication methods, spraying has been mostly investigated because of its portability, simplicity, and flexibility on various large-area substrates; in contrast to spraying, sputtering and dip coating methods require ultra-high vacuum facilities and thus entail costly DSSC applications [18].

The effectiveness of using a custom-made triple-chain surfactant, namely, 1,4-bis(neopentyloxy)-3-(neopentyloxycarbonyl)-1,4-dioxobutane-2-silphonate (TC14), as a good stabilizer of GO/rGO and natural rubber latex (NRL) has been described [19]. This surfactant provides triple interactions and helps prevent GO/rGO agglomerations in dispersion. In contrast to commercially available sodium dodecyl sulphate (SDS), TC14 allows high interactions between GOrGO and NRL matrix; as a result, the stability of GO/rGO is increased [20]. In our study, TC14 and SDS surfactant were used to improve the stability of rGO sheets. GO was initially synthesized through electrochemical exfoliation by utilizing both surfactants and then subjected to chemical reduction by using hydrazine hydrate at a ratio of 100:1. The effects of the surfactants were systematically evaluated on the basis of the properties of rGO-based CE and the performance in DSSC. The results revealed that the proposed simple rGO film preparation can be applied to produce low-cost CE with a high energy conversion efficiency for DSSC.

2. Experimental details

2.1. Chemicals

In the production of graphene, two pieces of high purity graphite rods (99.99%) (GoodFellow GmbH, Germany), with a diameter and length of 10 and 150 mm, respectively, were used in the electrochemical exfoliation method. For the synthesis of TC14 surfactant, the chemicals used including neopentyl alcohol (Acros Organics, 50 g), *trans*-aconitic acid (Sigma Aldrich, 100 g), toluene-4-sulfonic acid monohydrate (Merck, 1 kg), toluene (Merck, 17 L), silica gel (Acros Organics, 5 kg), diethyl ether (Chem AR, 2.5 L), petroleum ether 40–60 (Merck, 17 L), alugram sheets (Macherey Nagel, 1 box), ethanol (Merck, 25 L), sodium bisulfite (Friendemann Schmidt, 1 kg) and methanol (Merck, 25 L). Meanwhile, hydrazine hydrate (Merck, 80% soluble in water) was used as a reducing agent. Fluorine-doped tin oxide (FTO)-coated glass substrate (Sigma-Aldrich) was used as substrates.The TiO_2 photoanode was prepared by mixing of 0.3 g of powder anatase TiO_2 (d = 25 nm), acetic acid and liquid anatase TiO_2 (d = 6 nm). The dye used was N719 purchased from Sigma Aldrich. Dimethyl-propyl-benzimidiazole iodide (DPMII) electrolyte was prepared from 0.6 M 1,2-dimethyl-3-propyl-benzimidiazole iodide (Sigma-Aldrich), 0.1 M

lithium iodide (Sigma-Aldrich), 0.5 M 4-*tert*-butylpyridine (Sigma-Aldrich), 0.1 M guanidine thiocyanate (QreC), 0.85 mL of acetonitrile (Sigma-Aldrich), 0.5 mL of valeronitrile (Sigma-Aldrich), and 0.05 M iodide (Sigma-Aldrich).

2.2. Preparation of reduced graphene oxide

GO was initially synthesized through electrochemical exfoliation in an electrolyte-containing surfactant by following the reported procedure [19,20]. The produced GO solution was further reduced to by using hydrazine hydrate at a volume ratio of 1:100 (hydrazine: GO) at 100 °C for 24 *h*.

2.3. Fabrication of dye-Sensitized solar cells

DSSC were fabricated by using a TiO_2 nanoparticle-coated FTO glass as a photoanode and an rGO-coated FTO as a CE. The standard preparation of photoanodes and electrolytes was described in detail in a previous study [21]. In this study, the photoanode with an area of 0.25 cm^2 was sensitized by immersing in N719 dye for 24 h. The prepared TC14-rGO solution was spray-coated with an airbrush onto a preheated FTO-coated glass substrate on a hot plate at 120 °C. The sandwich type DSSC was assembled by introducing the liquid electrolyte on the dye-sensitized TiO_2 film and then TC14-rGO counter electrode was clipped firmly with the photoanode and then used to study the photovoltaic performance.

2.4. Characterization techniques

The morphology of as-prepared samples were analyzed through field emission scanning electron microscopy (FESEM, Hitachi SU8020) and high-resolution transmission electron microscopy (HRTEM, FEI Tecnai F30). The spectral properites of the samples were accessed using MicroRaman spectroscopy (Renishaw InVia Raman Microscope), and UV–vis absorption spectroscopy (Agilent 8453 Spectrophotometer). Photovoltaic performance of the fabricated DSSC were evaluated by using a computer-programmed Keithley 2611 Source Meter under the illumination of simulated sunlight (100 mW cm^{-2}, AM 1.5) and a solar simulator (Oriel, 91160-100091192, Parccell Technologies) was used as a light source.

3. Results and discussion

Fig. 1(a–f) show the FESEM images of the TC14-rGO, TC14-GO, and SDS-rGO film samples. The FESEM micrographs in Fig. 1(a-b) reveal that the TC14-rGO sample is composed of large rGO sheets on the FTO glass. A transparent and wrinkled morphology is observed at the edge site (pointed by arrows). This observation is due to the isolated oxygen reaction sites, and the resultant defects are reduced during the chemical reduction of GO [20]. By comparison, the SDS-rGO sample (Fig. 1(c–d)) contains thicker sheets with slightly agglomerated rGO sheets than the other samples do. The uniformity of the TC14-rGO film is retained because of the formation of a well-dispersed and stable solution of rGO assisted by TC14. Compared with those in the TC14-GO sample (Fig. 1(e–f)), the graphitic structures are more densely pack with highly crumpled structures formed through oxidation. As previously reported, the distinct morphologies of the rGO sheets greatly influence the optical and photovoltaic performances [22,23]. The FESEM images are supported by the findings of HRTEM analysis.

The HRTEM images (Fig. 2(a–b)) reveal few rGO layers with large and transparent sheets observed in the TC14-rGO sample, which consists of approximately 2–4 layers. By comparison, the slightly blur image of the TC14-GO sample shows multilayer sheets at the edge site, and these sheets are formed through the insertion of various oxygen-containing functional groups during oxidation (Fig. 2(c)).Significant damages and slightly thick graphitic sheets are observed in the SDS-rGO sample (Figs. 2(d–e)). The intrinsic wrinkles are found in the calculated layers of approximately 5–6 layers of rGO. These findings indicate that the TC14-assisted rGO possesses a more stable wide-open rGO sheets, which may enhance the diffusibility of electrolytes in DSSC [17,18,24,25]. However, both rGO film samples do not alter the overall morphology of the graphitic sheets.

The Raman spectra [Fig. 3(a)] were examined to compare the TC14-rGO, TC14-GO, and SDS-rGO film samples and to confirm the successful reduction of GO to rGO by using hydrazine hydrate. Two prominent peaks, namely, D and G bands, are found in the spectra of TC14-rGO and SDS-rGO samples. These bands are located in the range of 1367.8–1432.7 and 1582.7–1587.9 cm^{-1}, respectively. I_D/I_G ratio is necessary to predict the existence of defects and sizes in sp^2 domains [26]. The I_D/I_G ratio of TC14-rGO is 0.69, and this value is lower than that of SDS-rGO (I_D/I_G = 0.80). This result is attributed to the presence of rGO functionalization-assisted by triple tail surfactant and the restoration of the sp^2 domain in the rGO structures after reduction is completed [27,28]. An increase in the I_D/I_G ratio of SDS-rGO suggests that graphitic domains are distorted [29,30] and rGO is exfoliated into a single-layer structure [31]. To calculate the number of layers of each rGO sample, we used the following equation: $\omega_G = 1581.6 + 11/(1 + n^{1.6})$ where ω_G is band position in wavenumbers and n is the number of layers present in the sample [32]. It is observed that the TC14-rGO and SDS-rGO samples contain approximately 2–4 layers and 5–6 layers, respectively, and these findings are consistent with those revealed through HRTEM. AFM was employed to confirm the thickness of TC14-rGO (Fig. 3(b)). The measured thickness of the rGO sheets is approximately 10–12 nm. This finding is consistent with the Raman result showing that the highest number of rGO layers is 10. The thickness of the rGO sheets is likely lower than that of pure GO because oxygen-containing functional groups and lattice defects are removed

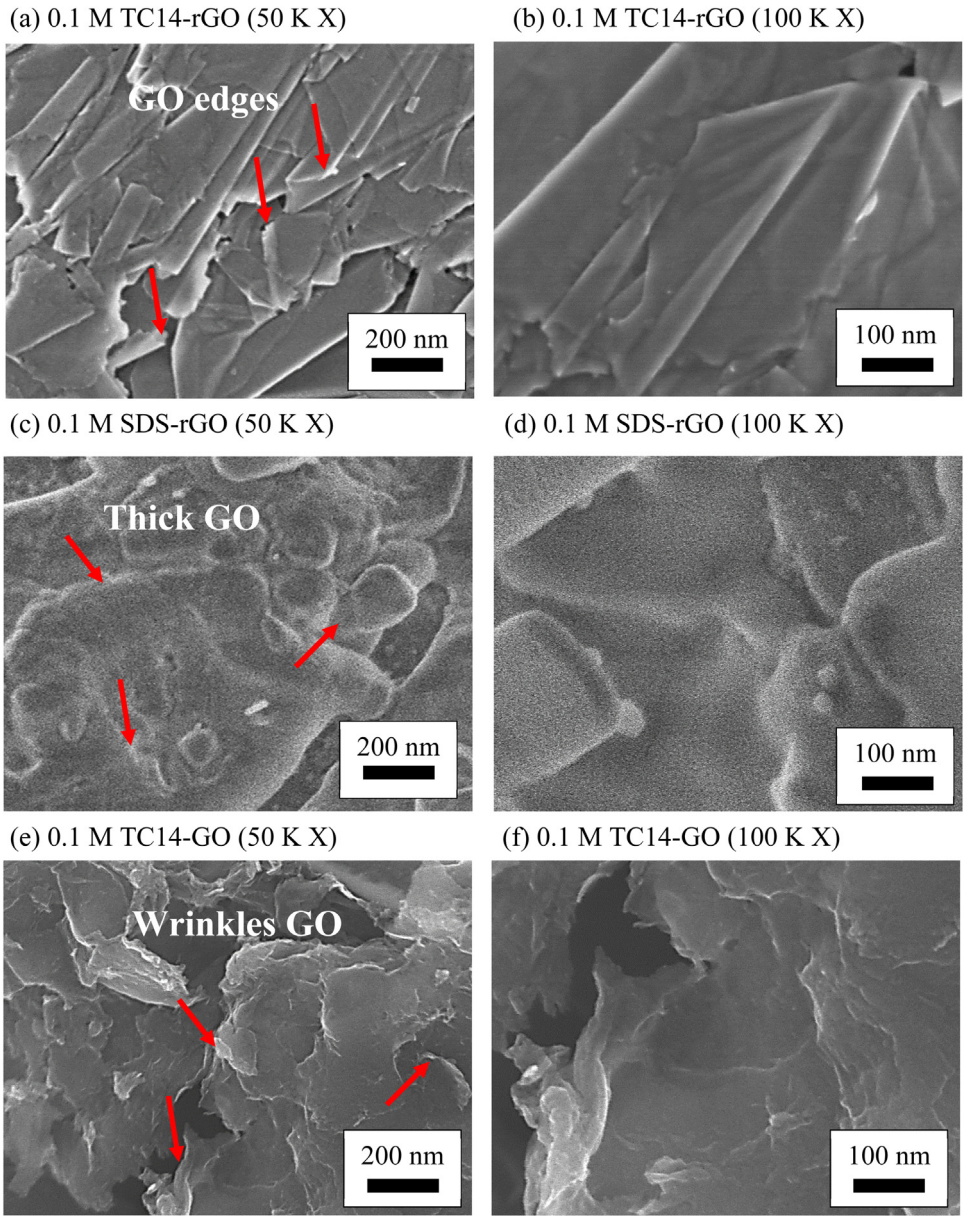

Fig. 1. FESEM images of (a)-(b) TC14-rGO, (c)-(d) SDS-rGO and (e)-(f) TC14-GO sheets.

during chemical reduction. The AFM result also confirmed that the rGO sheets are composed of thin and wrinkled sheets that helps to enhance the electrical, capacitance, optical, and optoelectronic properties.

The successful reduction of GO to rGO is also indicated by the transmittance values of the samples subjected to UV–vis analysis (Fig. 4). The prepared rGO films maintain an optical transmittance of approximately 80–95% in the range of 500–800 nm. At a wavelength of less than 500 nm, the TC14-rGO sample yields the highest transparency rate of up to 80%, and this value is higher than that of SDS-rGO film (60%). An increase in the restacking number of layers and non-continuous rGO particles of the sample-assisted by SDS surfactant may contribute to the lower transmittance of the obtained film [10]. Another possible reason is the greater solubility promoted by TC14. When sprayed, the rGO sheets less likely form bundles, which subsequently form a more dispersed and cohesive film that enhances the traveling light. However, the TC14-GO electrode generates a slightly lower transmittance of (< 85%) than TC14-rGO film does (∼90%). The high transmittance values of TC14-rGO at above 550 nm are probably attributed to the low restacking of graphite structures after reduction and annealing occur and thus allow light to travel on FTO films [33]. This finding confirms that the oxygen-containing functional group in GO is reduced by hydrazine hydrate treatment. Thus, several layers of rGO sheets are produced. This result is consistent with that described in a previous work revealing that the transmittance values increase as the number of layers decreases [10].

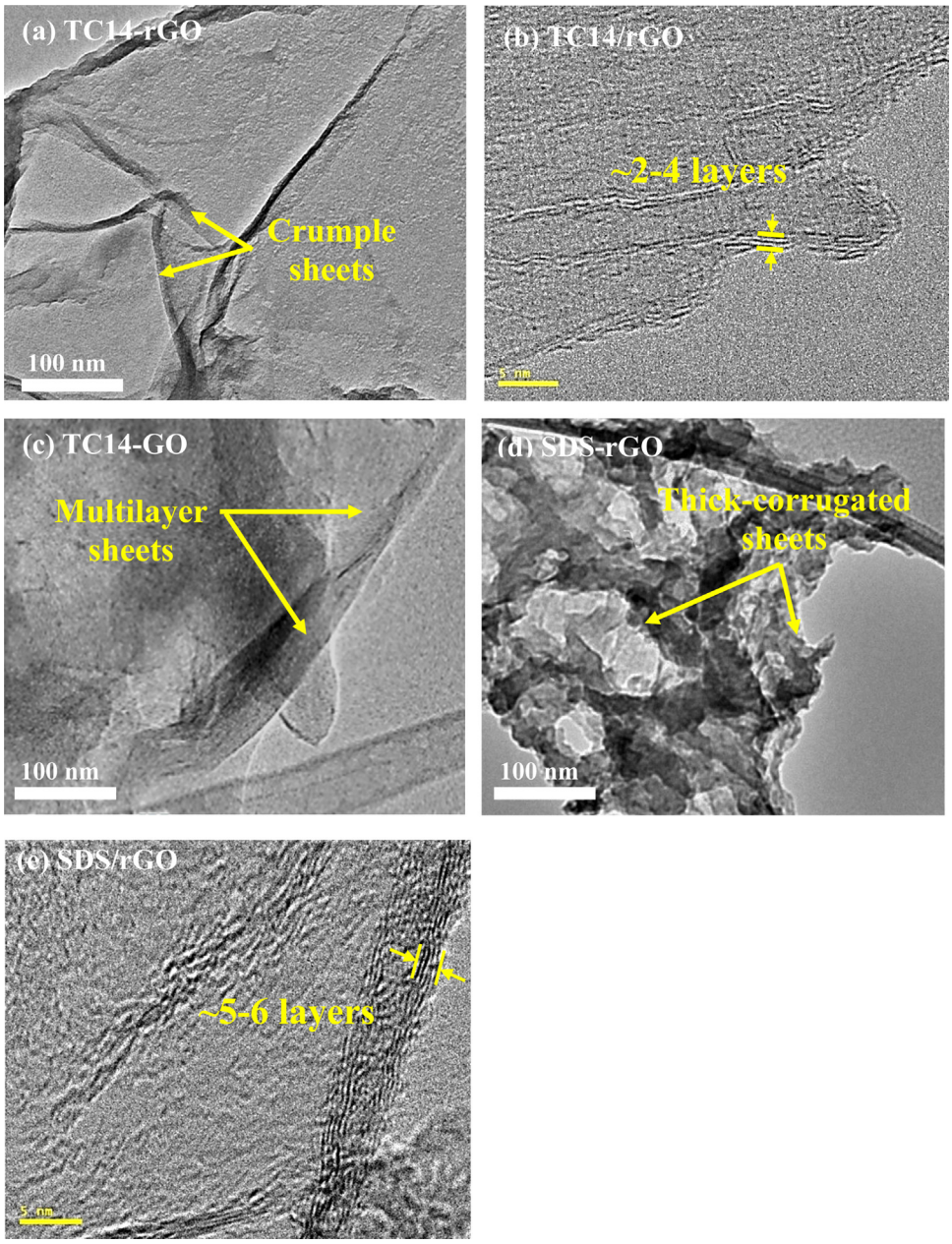

Fig. 2. HRTEM images of (a)-(b) TC14-rGO, (c) TC14-GO (d)-(e) SDS-rGO sheets.

The transmittances of TC14-rGO, TC14-GO, and SDS-rGO films do not significantly alter the transparency of FTO substrates [33,34].

The optical band gaps of TC14-rGO, TC14-GO, and SDS-rGO are determined on the basis of a Tauc plot [Fig. 4(b–d)]. Single-layer graphene yields a zero-energy band gap [35]. However, oxidation through electrochemical exfoliation has increased the zero energy band gap of graphene layers to approximately 3.94 eV. This finding is possibly caused by the insertion of various oxygen-containing functional groups between graphite layers [36]. After GO is reduced, the energy band gap of TC14-rGO and SDS-rGO is decreased to approximately 3.92–3.98 eV. This result indicates that the elimination of several oxygen-containing functional groups partially reduces from GO structures [37]. However the SDS-rGO sample shows the highest energy band gap of 4.06-4.20 eV due to the low stabilized single-tail SDS surfactant on the rGO structures as compared to rGO assisted by triple-tails TC14. These results are supported by MicroRaman analysis that revealed a small decrease in the I_D/I_G ratio from 0.82 for GO to ~0.60–0.80 for rGO samples; this decrease also corresponds to a slight decrease in defect density [38]. These observed band gaps in all of the samples indicate an intrinsic semiconductor.

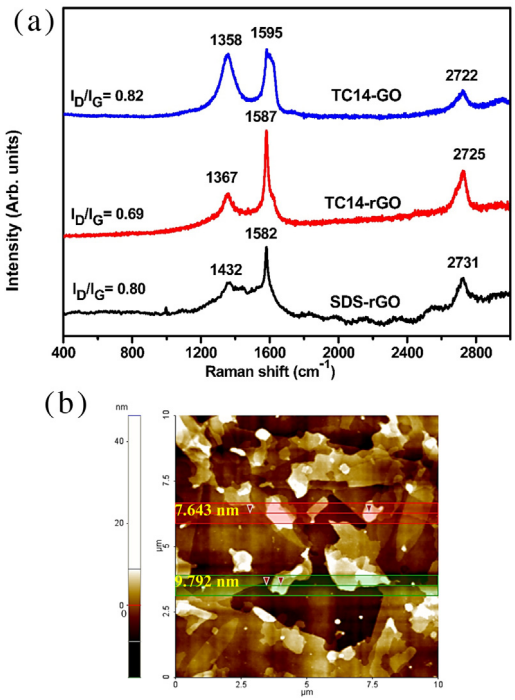

Fig. 3. (A) Micro-Raman spectra of TC14-rGO, SDS-rGO and TC14-GO sheets and (B) AFM of TC14-rGO sample.

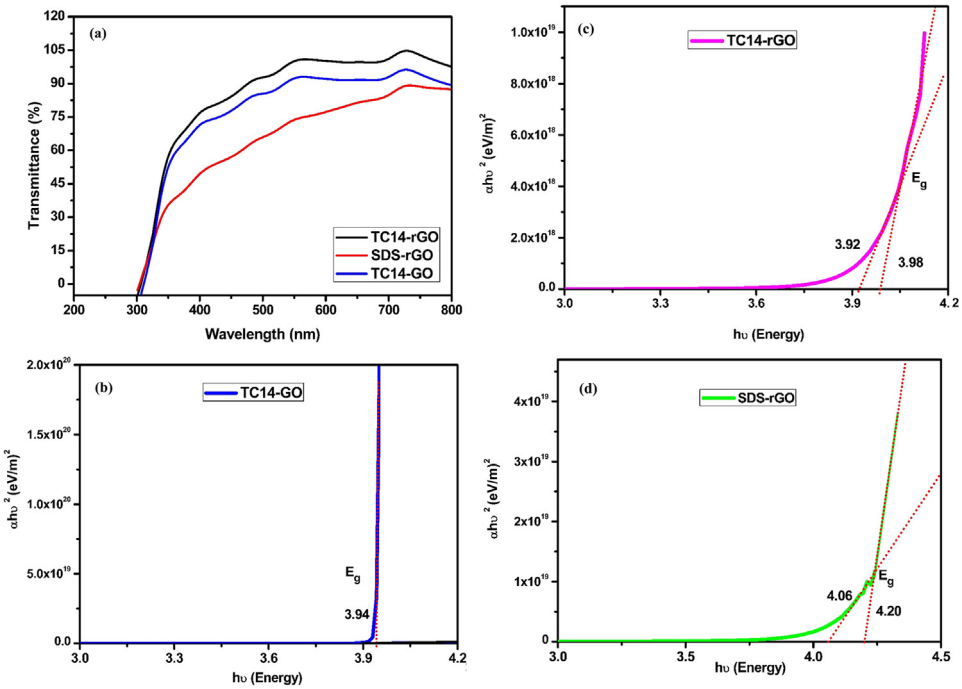

Fig. 4. UV–vis spectra and energy band gaps of TC14-rGO, SDS-rGO and TC14-GO sheets.

Fig. 5 compares the I–V curves of the TC14-rGO, TC14-GO, and SDS-rGO film samples. The TC14-rGO film exhibits the optimum I–V characteristics with the lowest resistance (R) of 3.0 Ω, followed by SDS-rGO with R of 3.4 Ω. By comparison, the TC14-GO film sample yields a slightly lower resistance (3.2 Ω) than the SDS-rGO sample does. This finding indicates that the use of TC14 plays a key role in stabilizing the graphitic sheets. Compared with SDS, TC14 facilitates an enhanced rGO

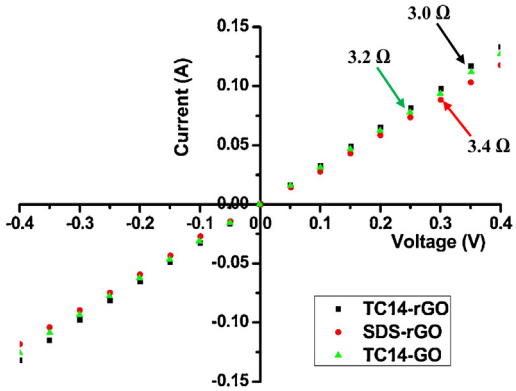

Fig. 5. *I-V* curve of TC14-rGO, SDS-rGO and TC14-GO sheets.

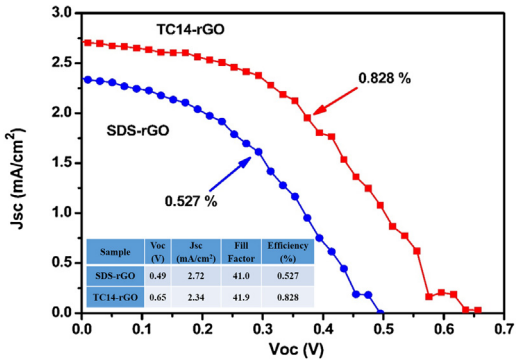

Sample	Voc (V)	Jsc (mA/cm²)	Fill Factor	Efficiency (%)
SDS-rGO	0.49	2.72	41.0	0.527
TC14-rGO	0.65	2.34	41.9	0.828

Fig. 6. *J-V* curves obtained for the TC14-rGO and SDS-rGO modified CE based DSSCs under the illumination of simulated solar AM 1.5G irradiation.

dispersion during exfoliation that causes a higher conductive film after TC14 is transferred on the substrate [18,24]. This result is consistent with that obtained in the MicroRaman analysis.

Fig. 6 illustrates the representative photocurrent density–voltage (*J–V*) curves of the DSSC with TiO_2 nanoparticles [19,39] as a photoanode and TC14-rGO, TC14-GO, and SDS-rGO film samples as a CE. V_{OC} of the TC14-rGO film (0.65 V) is higher than that of SDS-rGO film (0.49 V). The recombination rate and interfacial resistance are decreased because of the incorporation of a TC14-rGO film [40]. J_{SC} of the TC14-rGO sample (2.72 mA cm^{-2}) is higher than that of SDS-rGO (2.35 mA cm^{-2}) because of the enhancement of electron collection and transport facilitated by a high-bridging system from the TC14 and rGO sheets to the FTO substrate [41]. This observation indicates that the rGO-assisted TC14 surfactant contains more stable rGO sheets, which then enhanced the diffusibility of the electrolyte in the DSSC [18,24,25,42]. The TC14-rGO film sample also yields a slightly higher FF (41.9) than the SDS-rGO film sample does (41.0). This finding is consistent with the lowest resistance observed in the TC14-rGO sample (3.0 Ω). The low resistance of the rGO-assisted TC14 is correlated with the morphological characteristics of the rGO structures. The higher surface area of the TC14-rGO sample provides easy pathways for electron movement and thus improves the FF of CE. These characteristics of DSSC indicate that the rGO-assisted TC14 can increase the interfacial contact and electron half-life and decrease the charge recombination rate via the rapid path for the transport of electrons to the FTO glass [43]. By contrast, the rGO-assisted by SDS exhibits a slightly lower conversion efficiency (0.527%); this finding suggests that the sample contains a less affective area because of the single-tail-stabilized rGO on the FTO glass, which provides high surface resistance [24,44,45]. However, the efficiency of 0.828% of the TC14-rGO in DSSC is lower than that described in a previous report because of different fabrication processes and raw materials [25]. Therefore, the TC14-rGO CE with a high catalytic activity and an excellent electrical conductivity is favourable for high-performance DSSC.

The possible reason for the improvement in the power conversion efficiency of TC14-rGO film in DSSC as follows. Reduction is performed on the basis of a typical reduction growth mechanism of GO to rGO using hydrazine hydrate [28]. In particular, TC14 reduces the surface tension of the rGO sheets. As a result, the dispersion of rGO on the FTO film surface is enhanced. Reduction also contributes to the enhancement of the dispersion of single- and multi-layers of rGO sheets. Therefore, the improvement of charge transfer resistance between rGO sheets and electrolyte is probably due to the removal of excess oxygen-containing functional groups attached to the graphene sheets. The preheated rGO film samples also improve the structural properties of TC14-rGO sheets and the charge transfer between rGO sheets and electrolytes [46]. The low interaction between SDS and GO structures may produce few opening gaps and stacked layers. Thus, the highest resistance of the SDS-rGO film is obtained, as revealed by I–V measurement.

4. Conclusion

We have demonstrated a facile and low-cost preparation method for the fabrication of counter electrode for DSSC using reduced graphene oxide assisted byTC14 surfactant. This highly active and stable TC14-rGO modified CE based DSSC showed improvement in the J_{SC}, V_{OC}, and FF functions. By comparison, the TC14-rGO film sample yields a higher solar efficiency (0.828%) than the SDS-rGO film sample (0.527%) does when TiO_2 nanoparticles are used in photoanode. This finding indicates that the usage of TC14 surfactant is an efficient stabilizer to enhance rGO dispersion and thus improve photovoltaic performance. Therefore, this study can be used as a basis for the development of a new generation of high-performance and low-cost DSSC.

Acknowledgment

The authors would like to express their appreciation to the TWAS-COMSTECH Joint Research Grant (Grant code: 2017-0001-102-11), National Nanotechnology Directorate Division (2014-0015-102-03), Fundamental Research Grant Scheme (Grant code: 2015-0154-102-02) for their financial support.

References

[1] X. Xu, D. Huang, K. Cao, M. Wang, S.M. Zakeeruddin, M. Gratzel, Sci. Rep. (2013) 3.
[2] G. Hagfeldt, L. Boschloo, L. Sun, Kloo H. Pettersson, Chem. Rev. 110 (11) (2010) 6595–6663.
[3] S. Thomas, T.G. Deepak, G.S. Anjusree, T.A. Arun, S.V. Nair, A.S. Nair, J. Mater. Chem. A 2 (13) (2014) 4474–4490.
[4] M. Wu, X. Lin, Y. Wang, L. Wang, W. Guo, D. Qi, X. Peng, A. Hagfeldt, M. Gratzel, T. Ma, J. Amer. Chem. Soc. 134 (7) (2012) 3419–3428.
[5] S. Cho, S.H. Hwang, C. Kim, J. Jang, J. Mater. Chem. 22 (24) (2012) 12164–12171.
[6] H. Xu, X. Zhang, C. Zhang, Z. Liu, X. Zhou, S. Pang, X. Chen, S. Dong, Z. Zhang, L. Zhang, ACS Appl. Mater. Interface 4 (2) (2012) 1087–1092.
[7] C.B. Jacobs, T.L. Vickrey, B.J. Venton, Analyst 136 (17) (2011) 3557–3565.
[8] A.A. Arbab, K.C. Sun, I.A. Sahito, A.A. Memon, Y.S. Choi, S.H. Jeong, J. Mater. Chem. A 4 (4) (2016) 1495–1505.
[9] A. Badawi, N. Al-Hosiny, S. Abdallah, Superlattices Microstruct. 81 (2015) 88–96.
[10] M.K. Ahmad, C.F. Soon, N. Nafarizal, A.B. Suriani, et al., Optik 127 (2016) 4076–4079.
[11] J.N. Coleman, Acc. Chem. Res. 46 (1) (2013) 14–22.
[12] A. Kaniyoor, S. Ramaprabhu, J. Mater. Chem. 22 (17) (2012) 8377–8384.
[13] L. Qiu, H. Zhang, W. Wang, Y. Chen, R. Wang, Appl. Surf. Sci. 319 (2014) 339–343.
[14] J. Velten, A.J. Mozer, D. Li, D. Officer, G. Wallace, R. Baughman, A. Zakhidov, Nanotechnology 23 (8) (2012) 085201.
[15] C. Xu, J. Li, X. Wang, J. Wang, L. Wan, Y. Li, M. Zhang, X. Shang, Y. Yang, Mater. Chem. Phys. 132 (2) (2012) 858–864.
[16] D. Dodoo-Arhin, R.C.T. Howe, G. Hu, Y. Zhang, P. Hiralal, A. Bello, A. Bello, G. Amaratunga, T. Hasan, Carbon 105 (2016) 33–41.
[17] Q. Zhang, Y. Liu, Y. Duan, N. Fu, Q. Liu, Y. Fang, Q. Sun, Y. Lin, RSC Adv. 4 (29) (2014) 15091–15097.
[18] A. Jena, S.P. Mohanty, P. Kumar, J. Naduvath, V. Gondane, P. Lekha, J. Das, H.K. Narula, S. Mallick, P. Bhargava, Trans. Indian Ceram. Soc. 71 (1) (2012) 1–16.
[19] A.B. Suriani, M.D. Nurhafizah, A. Mohamed, I. Zainol, A.K. Masrom, Mater. Lett. 161 (2015) 665–668.
[20] A.B. Suriani, M.D. Nurhafizah, A. Mohamed, A.K. Masrom, V. Sahajwalla, R.K. Joshi, Mater. Des. 99 (2016) 174–181.
[21] E.S. Kwak, W. Lee, N.G. Park, J. Kim, H. Lee, Adv. Funct. Mater. 19 (7) (2009) 1093–1099.
[22] F. Barroso-Bujans, S. Cerveny, R. Verdejo, J.J. del Val, A. Alegra, J. Colmenero, Carbon 48 (4) (2010) 1079–1087.
[23] B. Tripathi, P. Yadav, K. Pandey, P. Kanade, M. Kumar, M. Kumar, Mater. Sci. Eng. B 190 (2014) 111–118.
[24] Y. Li, H. Wang, Q. Feng, G. Zhou, Z.-S. Wang, ACS Appl. Mater. Interface 5 (16) (2013) 8217–8224.
[25] A. Mohamed, A.K. Anas, A.B. Suriani, A. Azira, M. Sagiska, P. Brown, J. Eastoe, A. Kamari, N.H. Hashim, I.M. Isa, Colloid Polym. Sci. 292 (11) (2014) 3013–3023.
[26] J. Fan, S. Liu, J. Yu, J. Mater. Chem. 22 (33) (2012) 17027–17036.
[27] F. Tuinstra, J.L. Koenig, J. Chem. Phys. 53 (3) (1970) 1126–1130.
[28] Q. Xiang, J. Yu, M. Jaroniec, J. Phys. Chem. C 115 (15) (2011) 7355–7363.
[29] S. Stankovich, D.A. Dikin, R.D. Piner, K.A. Kohlhaas, A. Kleinhammes, Y. Jia, Y. Wu, S.T. Nguyen, R.S. Ruoff, Carbon 45 (7) (2007) 1558–1565.
[30] M. Ghislandi, E. Tkalya, A. Alekseev, C. Koning, G. De With, Appl. Mater. Today 1 (2) (2015) 88–94.
[31] L.C. Sim, K.H. Leong, S. Ibrahim, P. Saravanan, J. Mater. Chem. A 2 (15) (2014) 5315–5322.
[32] C.-H. Tsai, C.-H. Chen, Y.-C.Y. Hsiao, P.-Y. Chuang, Org. Electron. 17 (2015) 57–65.
[33] M. Wall, The Raman Spectroscopy of Graphene and the Determination of Layer Thickness, Thermo Scientific [Enligne], 2011 (Available:) https://tools.thermofisher.com/content/sfs/brochures/AN52252_E%201111%20LayerThkns_H_1. pdf.
[34] R. Cruz, D.A.P. Tanaka, A. Mendes, Sol. Energy 86 (2) (2012) 716–724.
[35] H.-S. Jang, J.-M. Yun, D.-Y. Kim, D.-W. Park, S.-I. Na, S.-S. Kim, Electrochim. Acta 81 (2012) 301–307.
[36] Z.-Y. Li, M.S. Akhtar, J.H. Kuk, B.-S. Kong, O.B. Yang, Mater. Lett. 86 (2012) 96–99.
[37] M.S. Poorali, M.M. Bagheri-Mohagheghi, J. Mater. Sci: Mater. Electron. 27 (1) (2016) 260–271.
[38] H.C. Hsu, I. Shown, H.Y. Wei, Y.C. Chang, H.Y. Du, Y.C. Chang, et al., Nanoscale 5 (1) (2013) 262–268.
[39] M.K. Ahmad, V.M. Mohan, K. Murakami, J. Sol-Gel Sci. Technol. 73 (3) (2015) 655–659.
[40] G.S. Han, S. Lee, E.S. Yu, S.P. Park, I.S. Cho, H.S. Jung, J. Electrochem. Soc. 163 (6) (2016) 469–473.
[41] Y.B. Tang, C.S. Lee, J. Xu, Z.T. Liu, Z.H. Chen, Z. He, Y.L. Cao, et al., ACS Nano 4 (6) (2010) 3482–3488.
[42] M. Motlak, N.A.M. Barakat, M.S. Akhtar, A.M. Hamza, A. Yousef, H. Fouad, O.B. Yang, Ceram. Int. 41 (1) (2015) 1205–1212.
[43] H. Wang, S.L. Leonard, Y.H. Hu, Ind. Eng. Chem. Res. 51 (32) (2012) 10613–10620.
[44] H. Choi, H. Kim, S. Hwang, Y. Han, M. Jeon, J. Mater. Chem. 21 (21) (2011) 7548–7551.